# IoT-Enabled Methane Monitoring and LSTM-Based Forecasting System for Enhanced Safety in Underground Coal Mining

SOUMYADEEP PATY

Department of Mining Engineering, Kazi Nazrul University, Asansol, West Bengal, India, mining.soumyadeep@knu.ac.in

Centre for IoT and AI Integration with Education-Industry-Agriculture, Kazi Nazrul University, Asansol, West Bengal, India, mining.soumyadeep@knu.ac.in

ARINDAM BISWAS

Department of Mining Engineering, Kazi Nazrul University, Asansol, India, mailarindambiswas@yahoo.co.in

Centre for IoT and AI Integration with Education-Industry-Agriculture, Kazi Nazrul University, Asansol, West Bengal, India, mailarindambiswas@yahoo.co.in

SUPREETI KAMILYA

Department of Computer Science and Engineering, BIT Mesra, Ranchi, Jharkhand, India, kamilyasupreeti779@gmail.com

SONIA DJEBALI

De Vinci Research Center, Courbevoie, France, sonia.djebali@devinci.fr

GUILLAUME GUERARD

De Vinci Research Center, Courbevoie, France, guillaume.guerard@devinci.fr



Ensuring safety in the mining industry is a critical concern for a nation's industrial advancement. Industry 4.0, characterized by the integration of advanced technologies, is at the forefront of efforts to enhance mining practices. Coal seams contain a range of hydrocarbon gases, predominantly methane, which is released in significant quantities during mining operations. Effectively mitigating methane emissions is imperative. The inclusion of methane forecasting allows for the early identification of potential methane emissions, hence results in significance enhancement in mine safety. The research work is focused on real-time remote monitoring and cloud-based forecasting of methane levels in underground coal mines. An Industrial Internet of Things (IIoT) device is developed for data acquisition in underground coal mines, capturing essential parameters such as methane concentration, temperature, and humidity. The collected data are utilized to train LSTM based multivariate forecasting model. The trained model is subsequently deployed in the cloud. The experiment is performed in a mine of Eastern Coalfields Limited, India. After the deployment of the proposed model, the developed IIoT device transmits real-time data, obtained from the mine, to the cloud. Based on the real time data, our model conducts methane forecasting and communicates results back to the IIoT device. The device issues immediate alerts when methane levels surpass predefined thresholds. This ensures enhanced safety in mining operations by providing warnings for both current and forecasted methane concentrations. The forecasted methane concentrations, along with real-time data, are accessible through mobile applications and a web-based dashboard. The accuracy of the proposed model is measured by mean absolute error, mean absolute percentage error and root mean square error, which demonstrate values of 156.95 ppm, 4.23% and 191.53 ppm respectively. A comparative study is performed where our model is evaluated against the multivariate Multilayer Perceptron (MLP), Vector autoregression (VAR) and Auto-Regressive Integrated Moving Average (ARIMA) models. The comparative study demonstrates that our developed model outperforms the others, showing superior results.

**Keywords:** Methane Monitoring, IIoT, Gas Sensor, LSTM Forecasting, Industry 4.0, Underground Mine Safety


ACM 2691-1914/2024/11-ART
http://dx.doi.org/10.1145/3703460

## 1 Introduction

Mining plays a pivotal role in a nation's progress, serving as a cornerstone for development. Among the diverse array of resources, coal emerges as a crucial asset due to its role as an economical energy source. Hence, the extraction of coal emerges as a critical undertaking. This process predominantly unfolds through two approaches: surface mining and underground mining. The latter becomes especially crucial when coal deposits are situated at greater depths, making underground coal mining the most feasible choice.

The safety measures in mining are of utmost importance for the protection of the lives and well-being of the personnel working in these conditions. Additionally, mining accidents can lead to substantial economic losses for both mining companies and the broader economy, and they also have a significant impact on the environment. Notably, coal seams have trapped various hydrocarbon gases such as methane, ethane, and propane since their formation, with methane being the most abundant among them. As a result, coal mining operations release a substantial amount of methane [1]. Surface mines generally have a minor impact as methane readily dissipates into the surrounding atmosphere. However, the situation shifts within underground coal mines [2]. Here, the removal of methane becomes essential, necessitating the implementation of sophisticated *artificial ventilation* systems. In this study, we define an artificial ventilation system as the mechanical process that introduces fresh air into mines and extracts air using a ventilator. This system, also known as mechanical ventilation, is crucial for removing gases released from mine strata, as well as other pollutants produced by machinery and human activities within the mines. On the other hand, natural ventilation is always present in mines. So, in case of the absence of artificial ventilation, a low amount of air flow is present because of the natural ventilation, that is not sufficient to remove the methane gas from mines.

This process plays a key role in maintaining safe working conditions for miners and preventing the build-up of methane, which can pose significant health risks and explosion hazards. Additionally, increased temperatures caused by heat from the surrounding geological layers and machinery operations add an additional dimension of risk for methane explosions, impacting the well-being and safety of underground miners. Because, raising the temperature of a methane-air mixture significantly expands its explosion range; specifically, it lowers the lower explosive limit (LEL) while raising the upper explosive limit (UEL) [3].

Smart mining within the context of Industry 4.0 arises from the intersection of cutting-edge information technologies (IT 4.0) and the mining sector, sparking innovation. The mining industry is experiencing profound changes, many efforts are underway that apply Industry 4.0 principles to enhance mining safety [4,5].

To address the safety issue concerning methane explosion, a number of works have been done in [6–8]. In [6], the authors have created a coal mine monitoring system using ZigBee-based wireless sensor nodes, which are equipped with multiple sensors for monitoring methane concentrations in the mine environment. In various studies [7, 9], scientists have utilized a range of gas sensors to identify the presence of hazardous gas leaks in mines, thereby enhancing worker safety.

The researchers of the study [10] have introduced a cloud-computing framework designed for wearable devices worn by miners during their underground operations. Through their innovative framework, they have effectively showcased the importance of such systems by enabling real-time monitoring of the underground work environment. Additionally, [11] have put forth an automated system aimed at creating a monitoring and operational management platform for underground mines. This system seamlessly integrates various technologies, including Wireless Sensor Networks (WSNs) and Geographic Information Systems (GIS).

While the previously mentioned studies primarily concentrated on methane monitoring, our current work goes a step further by aiming to achieve real-time remote monitoring and cloud-based forecasting of methane levels. The inclusion of methane forecasting allows for the early identification of potential methane emissions. Consequently, ventilation systems can be promptly adjusted to eliminate excessive methane from underground mines. In more challenging situations, this forecasting capability enables the timely withdrawal of personnel from the mines, ultimately contributing to the preservation of human lives.

Conventional methane forecasting models rely on empirical and numerical approaches [12–15]. However, these models often fall short in delivering high accuracy. In pursuit of enhanced precision, our current investigation adopts the Long Short-Term Memory (LSTM) algorithm, a deep learning-based approach. Deep learning widely embraces the LSTM neural network architecture due to its prevalence and effectiveness [16]. Our findings demonstrate that this approach yields promising results in forecasting methane levels.

To ensure the proper training of the deep learning-driven LSTM model, a substantial volume of data is required. In this study, we have developed an Industrial Internet of Things (IIoT) device for data acquisition from an underground coal mine. Our device comprises a wireless microcontroller unit, a methane sensor, a temperature and humidity sensor. The methane sensor, utilized in this study, represents an improved iteration of the sensor referenced in [17]. The original sensor, as detailed in [17], exhibited a drawback wherein it generated air turbulence around the sensing elements, resulting in unstable methane concentration readings. In our work, the modified version of the sensor effectively addresses and rectifies this issue. The developed device systematically collects data such as, methane concentration, ambient temperature and humidity levels. The collected data are subsequently utilized to train the multivariate forecasting model. The trained model is then deployed to the cloud.

In the concluding phase of our experiment, the device transmits real-time data to the cloud. Within the cloud infrastructure, our deployed model conducts methane forecasting and subsequently relays the forecasting results back to the IIoT device. Based on these forecasting results, the device is equipped to issue a warning alarm if the methane concentration surpasses a predefined threshold level. Furthermore, it is programmed to trigger an alarm if the real-time methane concentration also exceeds the established threshold level. The forecasted methane concentration results, along with real-time data, are accessible through mobile applications and a web-based dashboard provided by a third-party cloud service.

The rest of the paper is organized as follows. Section 2 describes the background study on the effects of methane in underground coal mines, sensor and IIoT technologies used for methane monitoring and the classical models used for methane forecasting. The methodologies of the proposed work along with the materials used are described in Section 3. Section 4 shows the results of the proposed work. Finally, the conclusion is given in Section 5.

## 2 Background

The study's background is derived from a broad range of literature, systematically presented and discussed to offer a thorough comprehension of the research context, as elaborated in the following subsections.

### 2.1 Effects of Methane in Terms of Safety in Underground Coal Mines

Methane ranks among the prevalent gases found within coal seams. It forms as a result of bacterial and chemical activity during the coal seam's formation and remains trapped within the coal seam since its inception, only to be liberated when the coal is broken during mining [1]. After liberation it may also accumulated within fractures, and less ventilated areas near roof, remains dormant until disturbed by mining activities. While not inherently toxic, its perilous nature stems from its ability to create explosive mixtures when combined with air. This propensity for methane explosions in underground coal mines represents a grave and potentially lethal threat to miners' safety [18]. Methane-related incidents consistently rank as the leading cause of fatal accidents within coal mines. Statistically, these accidents comprise roughly 40% of all incidents in coal mines, and the casualties resulting from methane incidents contribute to over 30% of the total fatalities in such accidents [19].

The article [20] examines methane explosions in Polish mines from 2013 to 2018, comparing them with global incidents. It outlines explosion prevention and methane control strategies in Polish coal mining, highlighting the need to harmonize these with other ventilation-related hazards, such as spontaneous coal combustion. Effective longwall panel design requires integrating predictions of methane emissions and other potential ventilation issues. The study in [21] explores forecasting daily average methane concentrations at two points in a Polish mine's longwall roadways: up to 10 meters in front of the wall and at the roadway's outlet. Using prognostic equations and ventilation data, the study compares methane levels at these locations. Results show similar accuracy in forecasts, although predictions are slightly less precise 10 meters from the wall face compared to the roadway outlet.

The liberation of methane due to coal breakage during mining operations raises valid concerns regarding the adequacy of ventilation systems necessary to ensure safety of underground mining environment [22-23]. Numerous mining and geological factors have the potential to influence the quantity of methane emitted from coal. The level of methane emission undergoes dynamic fluctuations in response to mining and geological activities.

Moreover, the author of [22] enumerates key parameters that exert the most significant influence on methane release within coal mines. These include the coal seam's level of maturation or rank of coal, its depth below the surface, the operational speed of face machineries such as conveyors and loaders, as well as the presence of degasification measures.

When methane and oxygen combine in specific concentrations, they form a potentially flammable or explosive mixture. Methane will burn smoothly when its concentration is below 5% when in contact with a thermal source. However, when the concentration ranges between 5.0% and 15%, methane and air create an explosive mixture. The most potent explosion occurs when methane is present at a 9% concentration with oxygen content exceeding 12%. This particular concentration is referred to as stoichiometric. Beyond a methane concentration of 15%, the mixture becomes flammable. It's worth noting that for any of these scenarios to occur, an energy impulse is required. The precise boundaries of these explosion conditions are illustrated in the Coward methane explosion triangle, as shown in Figure 1 [24].

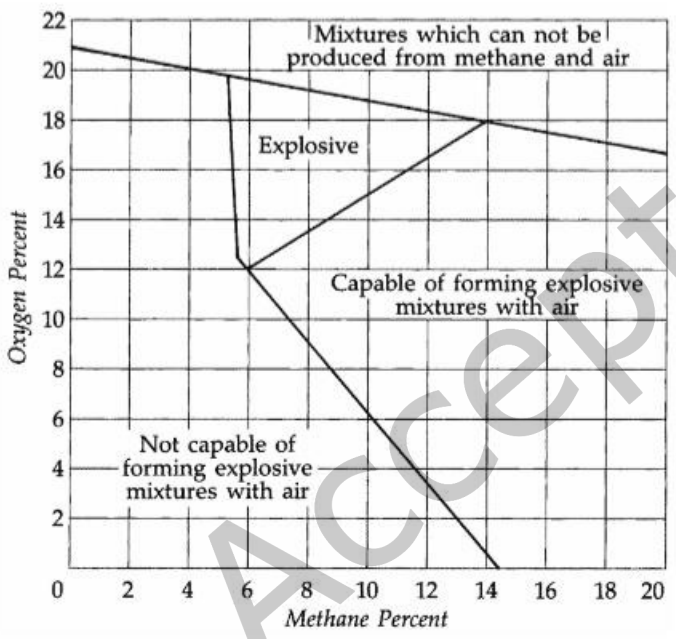


Figure 1: Relationship Between Quantitative Composition of Methane and Air with Explosibility [24]

The ABC triangle serves as a critical marker, defining the concentration range where methane can form an explosive mixture. Outside this triangle, mixtures either lack sufficient methane or oxygen to become explosive. Importantly, it's not possible to create a methane-air mixture within the area above the explosion triangle. The composition of the mixture within a particular space can change dynamically. This transformation can occur due to factors like adjusting air supply to mining areas, modifying the ventilation system, reorganizing mining processes, or altering exploitation techniques.

Furthermore, it's crucial to recognize the substantial impact of pressure and temperature on methane's combustibility. In terms of pressure, the influence on methane's explosiveness remains fairly consistent when operating under reduced pressure conditions. However, at elevated pressures, noteworthy changes occur. Specifically, the lower explosive limit (LEL) decreases, meaning that less methane is required for ignition, while the upper explosive limit (UEL) significantly widens, necessitating a higher concentration

of methane for potential explosion. Regarding temperature, its effect on methane's explosiveness is more moderate. At extremely low temperatures, like -110°C, the LEL stands at 5.6% CH4, meaning that a relatively higher concentration of methane is needed to trigger an explosion. Conversely, at a relatively higher temperature, such as +100°C, the LEL is slightly lower at 4.8% CH4, signifying a somewhat lower methane concentration required for potential ignition [1].

In the pursuit of averting methane explosions within coal mines, a series of crucial precautions must be implemented. First and foremost is the imperative to prevent the accumulation of methane in the vicinity of the shearer drum, a task achievable through the enhancement of ventilation systems. Another essential measure involves the installation of water spray systems at each cutter or drilling bit. This strategic placement serves to cool the metal components when they come into contact with rock, thus effectively curbing the potential for frictional ignitions. Furthermore, proper planning of ventilation is essential to eliminate any zones of air recirculation in underground environments. This step ensures that fresh air continuously flows through the mine, preventing the build-up of methane concentrations. Also, an indispensable action involves optimizing the placement of methane detectors at the working face. By positioning these detectors in the most strategic locations, miners can promptly identify and respond to any methane presence, thereby bolstering safety measures within the coal mine.

According to the Coal Mines Regulations 2017 (CMR 2017) in India, there's a strict ceiling on methane concentration within any section of an underground coal mine, set at a maximum of 1.25%. If this limit is exceeded, immediate action is mandated. Electric power supply to all cables and equipment must be promptly shut off, and individuals not directly involved in ventilation operations must be swiftly evacuated from the area.

### 2.2 Sensor and IIoT Technologies used for Methane Monitoring in Coal Mines

The safety of coal mining relies heavily on the careful monitoring and measurement of methane concentrations. In the current landscape, several types of sensors are utilized for this crucial task, including catalytic combustion type sensors [25, 26], optical interference-based sensors [27], and spectral absorption-based sensors [28, 29]. Sensors employing optical interference methods present a significant advantage in their expansive measurement range and overall stability. However, a drawback lies in their need for manual observation of interference patterns during measurements and their inability to seamlessly translate optical interference signals into easily processed electrical data. Additionally, these sensors tend to have bulkier profiles, require frequent adjustments, and can be susceptible to interference from other gases. On the other hand, Spectroscopic absorption-based methane sensors, particularly non-dispersive infrared (NDIR) spectroscopy-based methane sensors, stand out for their superior performance, though they come with a relatively higher cost [30]. Yet, they make up for this with their compact design and low power consumption, making them an appealing choice for specific applications. In contrast, sensors rooted in catalytic combustion methods are celebrated for their simplicity and cost-effectiveness. While they are confined to measuring methane concentrations within the 0-4% range, this range generally suffices for monitoring methane in a regular coal mine environment. Their affordability allows for their widespread deployment across various points within the mine, ensuring comprehensive coverage.

Methane monitoring, facilitated by sensor technology, offers diverse approaches. These include spot monitoring, typically carried out with handheld instruments, and wired communication systems. However, spot monitoring presents a concern as it places miners at risk due to the challenging environmental conditions prevailing within underground mines. On the other hand, wired communication often encounters issues such as cable impairment and the impracticality of operational systems for underground maintenance. With the advancement of technology, a specialized solution has emerged in response to these challenges: Wireless Underground Sensor Networks (WUSNs), uniquely address the specific needs of this context [31]. Continuous monitoring and the generation of extensive datasets for training machine learning-based forecasting models have posed significant challenges, primarily due to technical limitations. This is where the Industrial Internet of Things (IIoT) steps in within the realm of Industry 4.0, assuming a pivotal role in accomplishing this very goal. IIoT, comprised of an extensive array of sensor devices, signal frequency labels, and signal recognizers, excels in efficiently identifying, locating, and tracking real-world objects in real-time. It harnesses a fusion of existing technologies including Wireless Sensor Networks (WSNs), computer network technology, signal frequency identification technology, and database technology, all orchestrated to achieve precise objectives, such as intelligent and secure mining practices [32,33].

In [34], the study focuses on predicting harmful gases in mines and enhancing underground coal mine safety through an Arduino-based environment monitoring and control system, integrated with IoT and cloud computing. The system's performance was tested in real conditions within a Southeast Asian mine. The results showed that the Arduino-based sensors are effective in monitoring underground mine safety, demonstrating sensor accuracy and system effectiveness. Furthermore, the overall response of the proposed system achieved a sensitivity of 87.5% and a positive predictive value of 77.7%.

A study is done in [35] on eastern coal mines where the authors have developed a communication system that facilitates data transmission between underground smart devices and surface monitoring systems. The system utilizes LoRa technology for through-the-earth wireless communication. A specialized smart device was created to monitor methane and carbon monoxide levels, collecting sensor data on gas emissions to continuously assess the mining environment. The authors of [6], engineered a ZigBee-Wireless Sensor Node-based monitoring system for coal mines. This system utilized multiple sensor nodes to monitor methane concentrations within the mining environment. In this setup, akin to traditional wireless sensor networks, nodes transmitted their sensed data to a centralized base station for further analysis and guidance. However, it was evident that this solution fell short of meeting the evolving demands of the mining industry.

In an effort to use IoT into the coal mining landscape while embracing the concepts of cloud computing and big data, a comprehensive safety system was conceived by the authors of [36]. This proposed system offers holistic oversight of mining operations, prioritizing safety measures. It actively serves mining operations by raising alarms for unsafe working conditions and even orchestrating rescues in emergency scenarios.

Furthermore, other researchers, documented in [6,7,9], have embarked on deploying various gas sensors to detect hazardous gas leaks within mines, thus ensuring the well-being of workers. Researchers of [10] proposed a cloud computing-based framework integrated with wearable devices worn by miners during their subterranean duties. Their framework effectively demonstrated the importance of such systems through real-time monitoring of the subterranean work environment.

In their exploration of the potential offered by technologies like IoT, WSN, and Artificial Neural Networks (ANN), researcher of [37] developed a methane monitoring system for underground coal mines. In this innovative scheme, they introduced an alarming system coupled with a miners' positioning system, employing sensors distributed throughout the mines to predict dangerous and life-threatening working conditions in proximity to miners through ANN applications.

Similarly, IoT and WSN technologies have been leveraged to design smart helmets, further enhancing miner safety and thereby increasing overall mining productivity [38–40]. These systems incorporate devices for sensing factors like temperature, humidity, air quality, and helmet removal to ensure comprehensive safety measures are in place.

### 2.3 Traditional Approaches for Predicting Methane Concentration in Underground Mines

Recognizing the critical nature of methane concentration surveillance in subterranean mining operations, numerous scholars have dedicated their efforts to crafting models for methane monitoring and forecasting systems. Since methane emissions are influenced by numerous factors, it is crucial to consider a wide range of parameters when forecasting methane concentration [41, 42].

Since 21$^{st}$ century, there has been a surge on the study of short-term forecasting of methane emissions based on methane concentration records in the mine monitoring system (see for reference [43, 44, 46]). Methane concentration forecasting models can be categorized into three types based on their approaches [45]. The first category employs the empirical approach, relying on data garnered through the observation of processes or phenomena. The second category, known as the numerical approach, entails the creation of physical models representing the system or process, subsequently employing numerical approximation to solve it. Finally, the statistical methods based on the collection and in-depth analysis of raw data, harnessing mathematical techniques to discern patterns and construct forecast models.

An evaluation of one-day average methane concentrations forecast model is developed in [44], where the average methane concentration from the previous day is a descriptive variable that aids in the selection of appropriate methane prevention strategies. Another study analyzing one-day forecasts of the maximum methane concentration in a tailgate of a longwall ventilated with a U system is presented in [46]. An empirical study in Poland, cited in [47], evaluated three methane prediction models in mines: dynamic methane-bearing capacity models, autoregressive daily average methane concentration models, and a cause-effect daily average model. The first model forecasts based on planned mining volumes and geological surveys, aiding in ventilation planning and methane hazard reduction. The second model, usable from the second day post-launch, requires only the previous day's methane levels for daily predictions. The third model, which involves a 28-day delay post-launch for data collection, allows

parameter adjustments based on initial measurements. Each model offers benefits tailored to different stages of mining operations.

The authors of [12] have formulated a model for forecasting methane emission rates (Equation 1), considering factors such as methane flow within the methane drainage system, methane concentration within the mine atmosphere, and the total methane content present in the coal seam. Their study drew upon historical annual data, specifically capturing methane concentration from underground coal mines located in the UK.

$$ME = LfP_w + \left((1.857 \times D) - (D - U) + RfP_t\right) \quad (1)$$

$P_w$ is annual coal production (in ton).
$P_t$ is total annual underground mine coal production (in ton).
$D$ is the cumulative mass of methane (in $m^3$).
$U$ is the quantity of methane utilized (in $m^3$).
$L$ is the emission rate for per ton of coal produced (in $m^3$/ton).
$R$ is the residual gas content (in $m^3$).
$f$ is the conversion factor to convert volume flow to mass flow.

Another model for estimating methane emissions (Equation 2), as introduced by [13], takes the form of a regression equation. This model delves into the intricate interplay between mine emissions, the methane content within coal beds, and the rate of coal production.

$$ME = 1.08 \times 10^{-7}(CP \times MC) + 31.44 - 26.76 \times DV \quad (2)$$

$CP$ is the annual coal production in ton.
$MC$ is the total methane contained in $m^3$ per ton of coal.
$DV$ is a step function.

As per the insights provided by [41], a time series comprises a sequence of data collected at consistent intervals over time. When this concept is harnessed for predictive purposes, previous observations serve as valuable inputs for forecasting future values of specific target variables. The techniques employed for such forecasting are diverse and can range from regression analysis and machine learning models to filtering algorithms.

For instance, [14] introduced an innovative early warning system tailored for the prediction of methane levels within an underground coal mine. The methodology adopted in this study involved a two-fold process. Firstly, Principal Component Analysis (PCA) was employed to identify the primary factors exerting influence on methane levels. Subsequently, an artificial neural network was utilized to forecast methane concentrations. The dataset incorporated several key parameters, including methane, humidity, pressure, wind, and temperature. To train the neural network, the authors opted for the Levenberg-Marquardt (LM) algorithm.

In their pursuit to forecast methane concentrations within an underground mine, a study in [15] employed neural network as their forecasting tool. The neural network relies on the radial basis function

as its foundation. Their study encompassed the consideration of seven pivotal factors, which affect the methane emission. The dataset comprised a comprehensive set of 300 methane data points obtained from a coal mine in China. To assess the model's performance, they employed the relative error metric, comparing predicted values with actual ones.

## 3 Materials and Methods

The proposed system is a well-thought-out assembly comprising a System on Chip (SoC) microcontroller board, a methane gas measurement sensor, a temperature and humidity measurement sensor, an informative LCD display, and a buzzer designed to detect excessive methane gas levels in underground environments. The primary goal was to develop a compact, cost-effective, and precise device capable of measuring methane concentration, ambient temperature, and humidity while relaying this data to the cloud. Additionally, it has been programmed with a dual alert mechanism to promptly notify users when predefined gas concentration thresholds are surpassed. The first alert is triggered audibly through a buzzer, ensuring that on-site personnel are immediately informed. Simultaneously, an SMS alert is dispatched to designated recipients, offering a remote notification mechanism that enhances safety protocols in response to elevated methane levels. Strategically positioned within an underground coal mine, these IIoT devices continuously monitor methane concentration, temperature, and humidity, contributing to enhanced safety and environmental awareness. The complete dataflow framework of this study is visually represented in Figure 2.

In addition, this innovative solution facilitates real-time and historical data monitoring through a web-based dashboard and a mobile application, all accessible via an internet connection. Beyond mere data collection, the cloud-based system incorporates LSTM based deep learning model that analyze the historical data, enabling the prediction of methane concentration in mine atmosphere within the mine for the next 2 hours, with hourly granularity. Users can conveniently access these forecasted methane concentration values through both web-based and Android applications, enhancing operational efficiency and safety in underground mining operations.

### 3.1 Proposed hardware setup of the IIoT device

For the proposed IIoT enabled device, the ESP32 WROOM board was selected as the hardware foundation. This board is renowned and widely adopted in the creation of IIoT applications. At its heart lies the ESP32-D0WDQ6 chip, which is a powerful component boasting two energy-efficient Xtensa® 32-bit LX6 microprocessors. The chip's internal memory configuration is impressive, comprising 448 KB of ROM dedicated to booting and core functions, alongside 520 KB of on-chip SRAM allocated for data and instructions. What sets this chip apart is its scalable and adaptive design. It houses two independently controllable CPU cores, with a flexible CPU clock frequency ranging from 80 MHz to 240 MHz. Moreover, the chip incorporates a low-power coprocessor that can efficiently handle tasks with lower computing demands, such as peripheral monitoring, thus conserving energy [48]. The ESP32 chip also boasts an extensive array of integrated peripherals, ranging from ADC, DAC, UART, I2S, and I2C interfaces. This versatile hardware platform serves as a robust foundation for the IIoT- based methane monitoring and forecasting device.

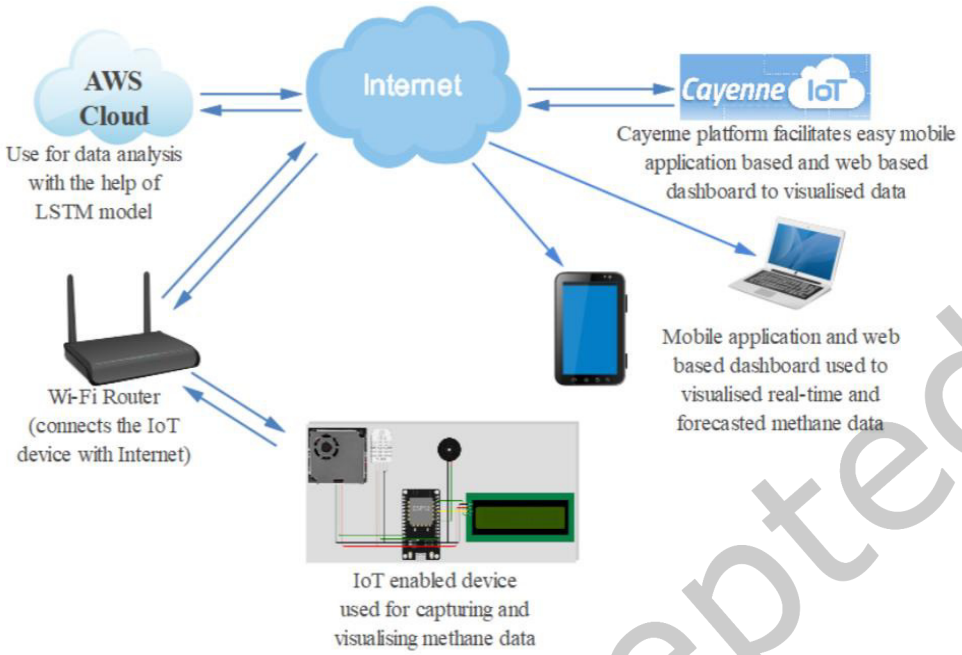


Figure 2: Visualization of the Comprehensive Dataflow Framework in the Study.

The methane sensor utilized in this study is founded on $SnO_2$ and was modified version of the sensor originally proposed by [16]. The fundamental material underpinning this sensor is $SnO_2$, complemented by the inclusion of a fan that plays a pivotal role in ensuring consistent airflow across the sensor. This particular sensor offers several advantages, including its cost-effectiveness, remarkable sensitivity, exceptional thermodynamic stability, and a notable capacity for adsorbing gaseous molecules. For more comprehensive insights into the sensor's specifications and calibration related details can be found in subsection 3.2.

The DHT-22, is a digital sensor designed for precise measurement of relative humidity and temperature. It relies on a capacitive humidity sensor and a thermistor to measure the environment temperature and outputs a digital signal via its data pin, eliminating the need for analog inputs. Its operational parameters include a 3-5V power range, a maximum current draw of 2.5mA, humidity measurement spanning 0-100% with an accuracy of 2-5%, and temperature measurement covering -40 to 80°C with an accuracy of ±0.5°C. On the other hand, the AM2302 is a calibrated digital module that offers accurate temperature and humidity readings through its advanced technology.

A 16×2 LCD 1602 display, interfaced through an I2C module, serves as the visual interface for presenting real-time methane, temperature, and humidity measurements, as well as alert messages within the system. Additionally, a piezoelectric buzzer is seamlessly integrated into the system, playing a crucial role in enhancing safety. The buzzer operates in two distinct modes: it issues a continuous, attention-

grabbing beep whenever methane levels surpass the stringent 1.25% regulatory limit, serving as an immediate warning for users. Moreover, it adopts a rhythmic signaling pattern, emitting a distinct beep at 5-second intervals if the forecasted methane concentrations for the upcoming 2 hours breach the critical 1.25% threshold, ensuring vigilant monitoring of potentially hazardous conditions.

The circuit's schematic diagram is thoughtfully illustrated in Figure 3(a). However, safety takes precedence in the demanding subterranean mining realm, prompting the adoption of an additional layer of protection. In this context, a flameproof enclosure serves as the ultimate safety measure, enclosing the entire device. Additionally, the encloser is wrapped in a double layer of aluminum foil to shield it from external heat sources, with the added benefit of reflecting radiant heat. This enclosure acts as a robust barrier, effectively reducing the risk of ignition by isolating the device's sensitive internal components from the methane-rich environment. For a visual representation, refer to Figure 3(b), which displays the final assembly of the IIoT device.

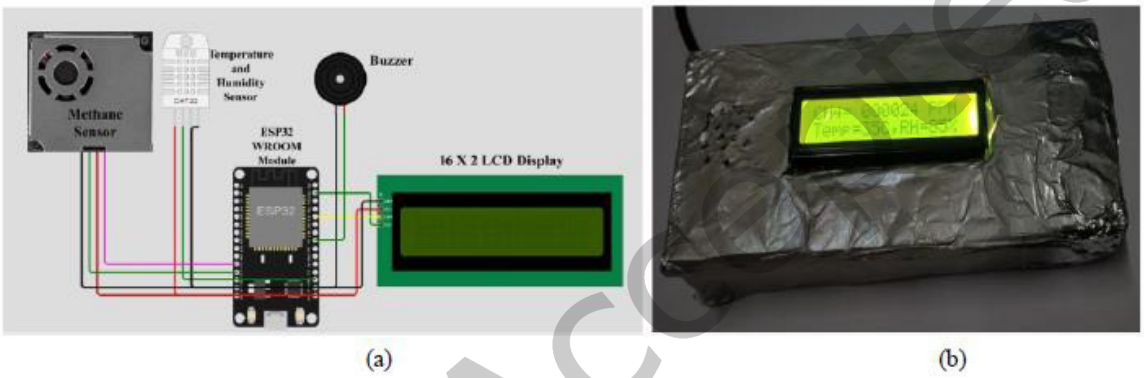


Figure 3: (a) Schematic diagram of the connections of components of IIoT device. (b) Final assembly of the IIoT device

### 3.2 Sensor Overview and Calibration

The sensor devised for this application is a cost-effective and lightweight passive resistor. It incorporates a resistive element consisting primarily of $SnO_2$, which is encased within Bakelite material. To provide its operating temperature, the sensor employs a nichrome heater enclosed within a plastic housing. Copper electrodes are affixed to this housing to facilitate electrical connections. The housing is further shielded by a stainless-steel mesh, providing an extra layer of protection against potential explosions, especially in scenarios where heater temperatures might reach hazardous levels. A small fan is put beneath the stainless-steel mesh to maintain a consistent airflow and ensure efficient cooling of the heater, preventing temperature spikes. In the original design of the sensor [16], the fan was positioned as a forcing type, leading to air turbulence that caused instability in methane readings. However, in this study, we have made a significant modification by relocating the fan to the outlet side, converting it into an exhaust type. This strategic adjustment effectively reduces air turbulence at the sensing material, resulting in more stable methane readings. To ensure its integrity, the entire system is enclosed within a chemically inert

and highly resilient aluminum oxide cylinder, measuring 20 mm in diameter and 25 mm in height. The sensor's schematic diagram is thoughtfully depicted in Figure 4.

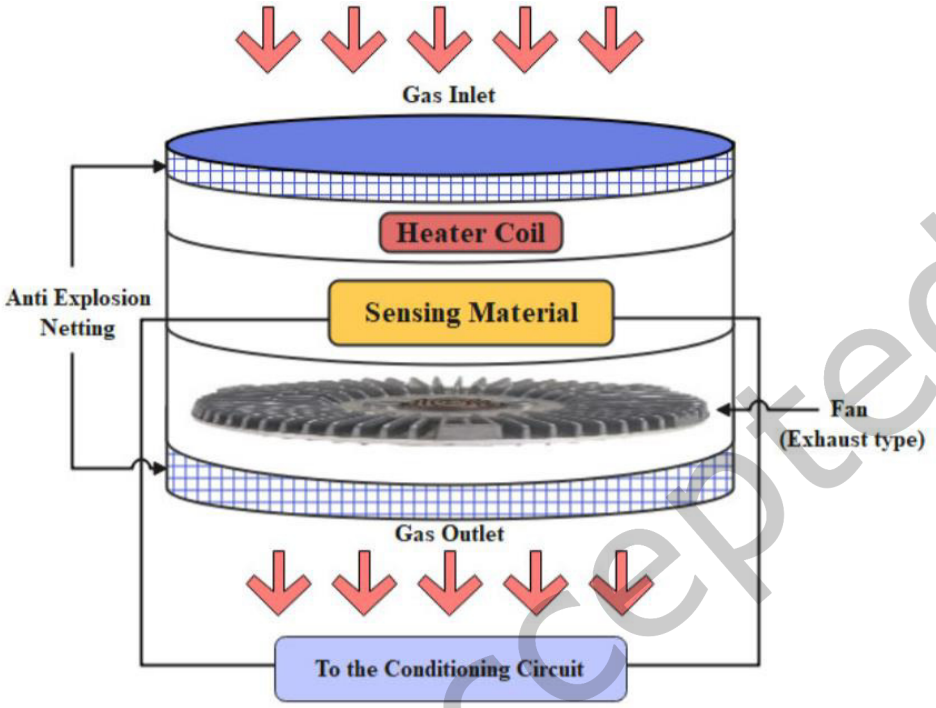


Figure 4: Schematic diagram of the $SnO_2$ based methane gas sensor

$SnO_2$ is selected as the foundational material for the sensor due to a host of advantageous attributes it possesses, encompassing its cost-effectiveness, heightened sensitivity, impressive thermodynamic stability, and notable capability to adsorb diverse gaseous molecules. Considering that heightened temperatures augment its responsiveness to a broad spectrum of gases, a nichrome heater has been thoughtfully incorporated into the sensor. Additionally, a fan has been included to ensure a consistent airflow and temperature within the system. An additional safety measure is the anti-explosion layer positioned atop the sensor assembly to eliminate any potential explosion risks arising from high temperatures. Under normal conditions with clean air, the sensor's resistance remains relatively stable. However, in the presence of methane in the air, it adsorbs onto the sensor surface, leading to a reduction in the $SnO_2$ material's resistance. Consequently, the concentration of methane in the air is determined by tracking the sensor's resistance alteration. A comprehensive overview of the sensor's specifications is presented in Table 1.

Based on the research conducted by Ghosh et al. [17], it has been established that there exists an exponential correlation between the methane concentration and the corresponding change in sensor resistance. This relationship is precisely described by Equation 3.

$$R_s = R_o e^{-K_1 C_s} \qquad (3)$$

Here, $R_s$ is considered as the resistance of the sensor (in ohm) at different methane concentrations, and $C_s$ as the methane concentration (in parts per million or ppm). $R_o$ denotes the resistance when the methane concentration is 0. $K_1$ is the constant.

Table 1: Specifications of the methane sensor

| Parameters | Specifications |
|---|---|
| Heating coil input voltage | 5.0 V |
| Coil resistance | 40 Ω |
| Heating coil power consumption | 600 mW. |
| $SnO_2$ Sensing material resistance | 10 kΩ - 50 kΩ |
| Fan voltage | 5V DC |
| Power consumption of fan | 2.5 W |
| Sensitivity | Greater than 0.78 at 1000 PPM methane |

The ESP32 WROOM module employed in this study has built-in ADC (Analog to Digital Convertor) channels explicitly engineered for the measurement of analog voltage signals within 0-3.3V range. A signal conditioning circuit is developed to serve the purpose of translating alterations in sensor resistance caused by the presence of methane into the voltage range of 0-3.3V. The schematic diagram of this conditioning circuit is presented in Figure 5.

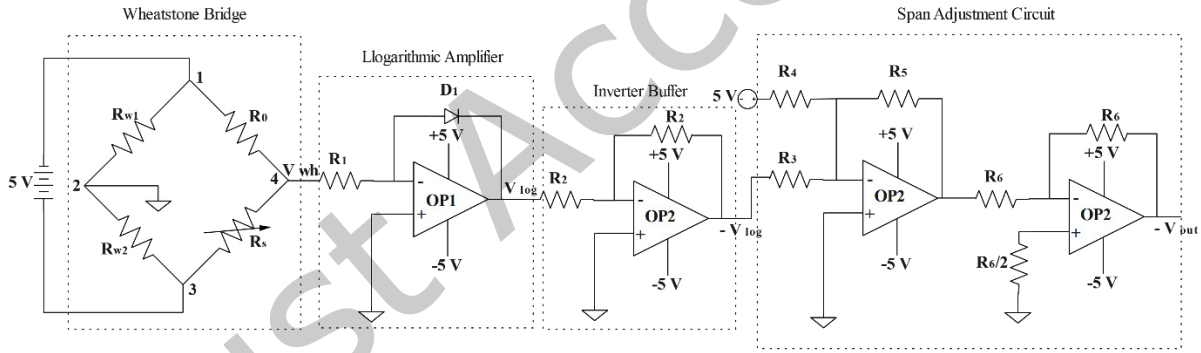


Figure 5: Schematic Representation of the Conditioning Circuit

The signal conditioning circuit comprises several key components, starting with a Wheatstone bridge responsible for measuring voltage changes corresponding to variations in sensor resistance. The voltage variation exhibits an exponential pattern, requiring the utilization of a logarithmic amplifier to transform this exponential voltage change into a linear one. Following this, a span adjustment circuit comes into play, ensuring that the output voltage is standardized within the 1–3.3V range. This standardized output can then be readily employed for industrial monitoring and control or transmitted as measurement data via the ESP32.

In this setup, the sensor is integrated into one arm of the Wheatstone bridge (designated as Rs), enabling it to measure changes in resistance linked to alterations in methane concentration within the air. To offset any resistance changes stemming from temperature or humidity influences, a resistor with resistance equivalent to the sensor's resistance in clean air (Ro) is placed in the adjacent arm of the Wheatstone bridge. The Wheatstone bridge configuration serves a dual purpose: not only does it convert resistance changes into suitable voltage variations, but it also enables compensation for any external factors' impact on resistance or voltage, such as temperature and humidity. Two fixed resistors Rw1 and Rw2 are placed in the other arms of the bridge write differently. Grounding at point 2 enhances the convenience of obtaining the output voltage resulting from the sensor's resistance change at point 4, which is subsequently fed into a logarithmic amplifier to change into a linear voltage, given that resistance change exhibits an exponential nature, as indicated by Equation 3. As terminal 2 is connected to ground, the voltage at terminal 2 is inherently set to zero. So, the voltage at terminal 4 in the Wheatstone bridge, denoted as $V_{wh}$, can be expressed by the equation provided below:

$$V_{wh} = \frac{R_s}{R_s+R_o} \times V_{in} \quad (4)$$

Here, $V_{in}$ is the input voltage (5 volt).

From the Equation 3 and 4 the following can be derived:

$$V_{wh} = \frac{e^{-K_1C_s} - e^{-2K_1C_s}}{1-e^{-2K_1C_s}} \times V_{in} \quad (5)$$

(1- $e^{-2K1Cs}$) can be approximated as 1 because $e^{-2K_1C_s} << 1$. So, the $V_{wh}$ can be approximated as,

$$V_{wh} = (e^{-K_1C_s} - e^{-2K_1C_s}) \times V_{in} \quad (6)$$

The voltage $V_{wh}$ is the output voltage from the Wheatstone bridge. This voltage is exponential in nature. To linearize this voltage, a logarithmic amplifier is employed. Output of the logarithmic amplifier $V_{log}$ can be expressed as:

$$V_{log} = -K_2 \ln\left(\frac{(e^{-K_1C_s} - e^{-2K_1C_s}) \times V_{in}}{I_s R_3}\right) \quad (7)$$

Here, $K_2$ represents a constant, expressed by Equation 8, where η stands for the emission coefficient, and $V_T$ denotes the thermal voltage of the diode implemented within the logarithmic amplifier. $I_s$ denotes the saturation current of the diode $D_1$.

$$K_2 = \eta V_T \quad (8)$$

The resulting voltage, denoted as $V_{log}$ and originally negative in polarity, undergoes a transformation by passing through an inverting amplifier to render it positive. Subsequently, this positive output traverses through a span adjustment circuit designed to regulate the voltage within the 1–3.3 V range. This adjustment serves the purpose of standardizing the voltage data. In this scenario, a concentration of 0 PPM methane corresponds to an output of 1 V, while 0 V signifies a fault in the sensor circuit. This standardization ensures a fail-safe system, distinguishing between a sensor failure or disconnection, both

of which the IIoT device interprets as a system fault rather than a zero-methane condition. Consequently, the zero concentration of methane is assigned a value of 1 V, while the maximum methane concentration value (in ppm), which is 15000 ppm in this context, is set to 3.3 V. Following its traversal through the inverting amplifier and the span adjustment circuit, the resultant output voltage, denoted as $V_{out}$, can be expressed as:

$$V_{out} = -K_3 V_{log} + K_4 \qquad (9)$$

The sensor undergoes calibration within a controlled laboratory environment, specifically a gas testing chamber designed for this purpose. Here, various known concentrations of methane are precisely introduced to the sensor, and the resulting output voltage, $V_{out}$, is recorded. For the calibration process, a series of methane concentrations were systematically employed, which includes 0 ppm (for fresh air), 500 ppm, 1000 ppm, 2000 ppm, 5000 ppm, 10000 ppm, 12500 ppm, and 15000 ppm. The visual representation of this laboratory setup for sensor calibration and testing the IIoT device is depicted in Figure 6.

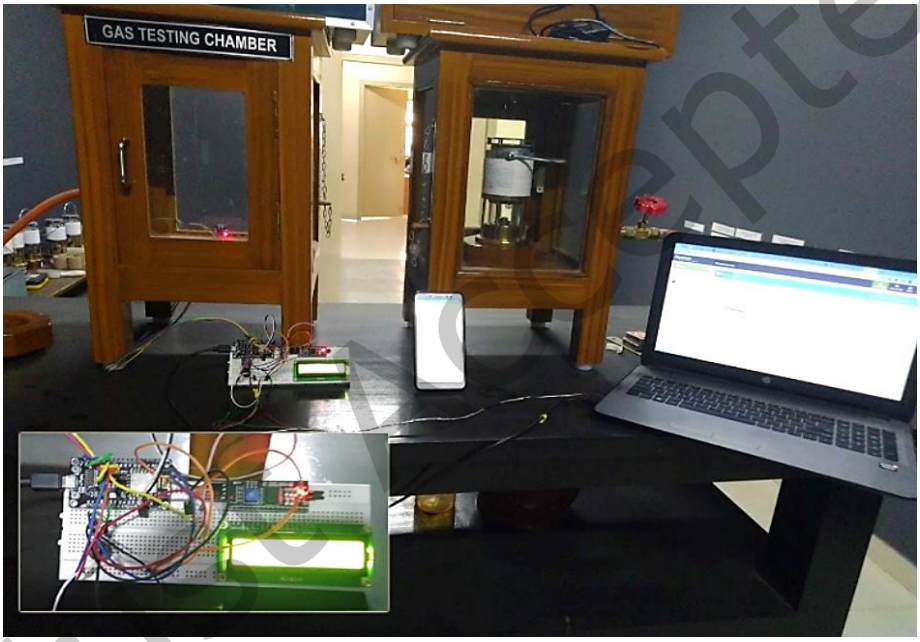


Figure 6: Laboratory setup for sensor calibration and the IIoT device testing

The *Vout* (in millivolts) obtained during calibration for various methane concentrations (in parts per million), as summarized in Table 2.

The relationship between the output voltage and different methane concentrations is then graphically presented in Figure 7. The calibration curve clearly demonstrates a linear relationship between the output voltage and methane concentration. The observed correlation exhibits a comparable linear nature to the theoretically derived relationship in Equation 9.

Table 2: Specifications of the methane sensor

| Methane Concentration (PPM) | *Vout* (millivolts) |
|---|---|
| 0 | 1000 |
| 500 | 1121 |
| 1000 | 1215 |
| 2000 | 1295 |
| 5000 | 1685 |
| 10000 | 2388 |

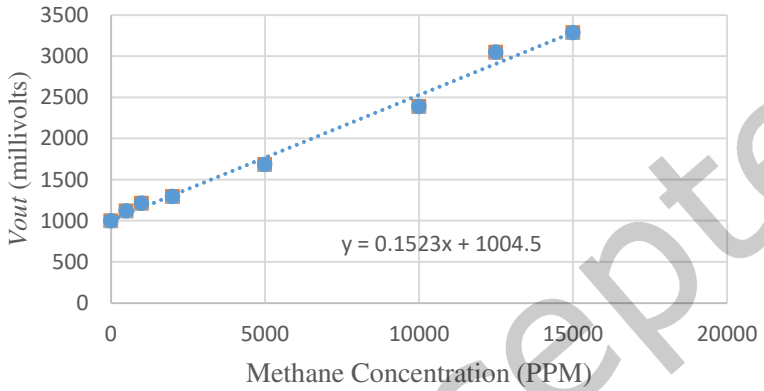


Figure 7: Calibration curve of the methane sensor

The experimentally established correlation between *Vout* and methane concentration in ppm is expressed in Equation 10, serves as empirical formula for methane concentration measurements facilitated by the developed IIoT device.

$$V_{out} = 0.1523 \times PPM + 1004.5 \qquad (10)$$

### 3.3 Gathering Historical Time-Series Data with the Developed IIoT Device

Extensive data is essential to train neural network-based forecasting models. However, readily available historical data is scarce in public repositories specially for all strategic location of an underground coal mine. To overcome this challenge, we deployed our developed IIoT devices strategically within an underground coal mine located in the eastern part of India. Specifically, it's part of the Eastern Coalfields Limited, India located at Raniganj Coalfield. The mine operates using a semi-mechanized bord and pillar system, employing Side Discharge Loaded (SDL) for coal loading and tubs for transportation. With two shafts, one for air intake and the other for return, ventilation is facilitated by a PV200 model main mechanical ventilator, operating on an exhaust ventilation system. The average airflow in the main return airway stands at 2320 cubic meters per minute and 1890 cubic meters per minute in the main intake airway. It's noteworthy that the mine seam holds a classification of a gassy seam of the third-degree coal

mine by Director General of Mine Safety (DGMS) standards, indicating that the emission rate of inflammable gas per ton of coal produced surpasses ten cubic meters.

These IIoT devices were strategically placed at three key locations: the coal mining face, the outbye side of the current mining panel, and the main return airway, as illustrated in the mining plan (refer to Figure 8).


Figure 8: Mine plan highlighting the location of the installed device

The current active mining panel is highlighted in green on the mine plan, as depicted in Figure 8. Moreover, it prominently marks the location of the IIoT devices using large red dots, labeled as location 1, 2, and 3, signifying their placement at the mining face, the outbye side of the working panel, and the return airway, respectively.

The forecasting model is trained independently by the datasets from these three distinct locations, and the training results are subsequently evaluated. Data was collected continuously for a duration of 100 days, spanning from mid-January to the end of April in 2023. This dataset encompasses information from both production shifts and maintenance shifts, providing a comprehensive source for training our models.

Generated dataset comprises three primary parameters: methane concentration in the mine air (expressed as a percentage), environmental temperature (measured in degrees Celsius), and environmental relative humidity (also presented as a percentage). These parameters are systematically recorded by the IIoT device at 30-second intervals and then locally stored at the edge. For the sake of data transmission efficiency and storage, the device calculates hourly averages for each parameter and subsequently transmits this aggregated data to the cloud via the MQTT protocol over TLS. This process yields a daily collection of 24 readings for each parameter per day, culminating in a comprehensive dataset of 2400 records for each parameter. A glimpse of the acquired average data, received by the cloud through MQTT protocol over TLS, is presented in Table 3, where the maximum methane obtained are highlighted for the three locations.

Table 3: A glimpse of the collected data using developed device

| | | Location 1 | | | Location 2 | | | Location 3 | | |
|---|---|---|---|---|---|---|---|---|---|---|
| Date | Time | Methane (PPM) | Temp. ($^o$ C) | Humidity (RH%) | Methane (PPM) | Temp. ($^o$ C) | Humidity (RH%) | Methane (PPM) | Temp. ($^o$ C) | Humidity (RH%) |
| 16-01-2023 | 18:00 | 3454 | 32.5 | 80.5 | 2527 | 30.5 | 73.1 | 2036 | 29.2 | 66.4 |
| 16-01-2023 | 19:00 | 4147 | 32.8 | 82.9 | 3196 | 31.6 | 75.2 | 2441 | 29.4 | 68.9 |
| 16-01-2023 | 20:00 | 3674 | 31.1 | 83.4 | 2956 | 29.6 | 76.9 | 1981 | 28.5 | 69.1 |
| 16-01-2023 | 21:00 | 2316 | 30.6 | 85.7 | 2383 | 29.4 | 78.2 | 1914 | 27.4 | 71.5 |
| 16-01-2023 | 22:00 | 2804 | 30.2 | 86.2 | 3408 | 28.6 | 79.3 | 2482 | 27.7 | 72.6 |
| 16-01-2023 | 23:00 | 4082 | 29.9 | 82.6 | 4194 | 28.9 | 75.5 | 3665 | 26.7 | 68.9 |
| 17-01-2023 | 00:00 | **4286** | 28.1 | 83.6 | **3965** | 27.4 | 76.7 | **3268** | 25.9 | 69.5 |
| 17-01-2023 | 01:00 | 3083 | 29.0 | 82.4 | 1757 | 27.9 | 75.4 | 1694 | 26.1 | 68.3 |
| 17-01-2023 | 02:00 | 1849 | 28.5 | 83.7 | 1693 | 27.3 | 76.8 | 1691 | 25.7 | 69.5 |
| 17-01-2023 | 03:00 | 2402 | 28.6 | 80.2 | 2463 | 26.4 | 73.2 | 1671 | 25.2 | 66.1 |

### 3.4 Designing of LSTM-Powered Time Series Forecasting Model for Methane Concentration

Multivariate time series analysis offers a viable approach for forecasting methane concentration in the atmosphere of underground coal mines. Drawing from existing literature and empirical models, it's evident that methane concentration is influenced by historical data of various factors such as environmental temperature, humidity, and other relevant variables. If we denote $y_{1,t}$ as the methane concentration at time t, and the dependent parameters at time t as $y_{2,t}$, $y_{3,t}$, ..., $y_{k,t}$, then the predicted methane concentration value at time *(t+h)* can be expressed through the following function.

$$y_{1,(t+h)} = f\left(y_{1,(t+h)}, y_{2,(t+h)}, y_{3,(t+h)}, \ldots\ldots\ldots\ldots, y_{k,(t+h)}\right) \qquad (10)$$

Advanced multivariate time-series analysis models are explored in this study through the incorporation of cutting-edge LSTM-based learning models from the field of machine learning. These LSTM models empower the construction of deep learning models with the capacity to delve deeply into complex and obscured patterns, thus enabling the forecasting of methane concentration by thoroughly scrutinizing the parameters impacting methane emissions.

Deep learning widely embraces the Long Short-Term Memory (LSTM) neural network architecture due to its prevalence and effectiveness. LSTM networks, which fall under the category of Recurrent Neural Networks (RNNs), represent a significant advancement over conventional RNN structures. The nature of the LSTM neural network used in the methane concentration forecasting model is specialized for handling sequences of data with potentially long-range dependencies. The superiority of LSTM network over standard RNN lies in the cell structure: while a standard RNN features just one threshold function, an LSTM network introduces four critical components within its hidden-layer structure, as illustrated in the accompanying figure 9. These are cell state, forgetting gate, input gate and output gate. These gates determine what data should be retained or forgotten over time, allowing the model to learn from sequences without losing crucial temporal details. This capability makes it adept at understanding patterns and trends of time series data.

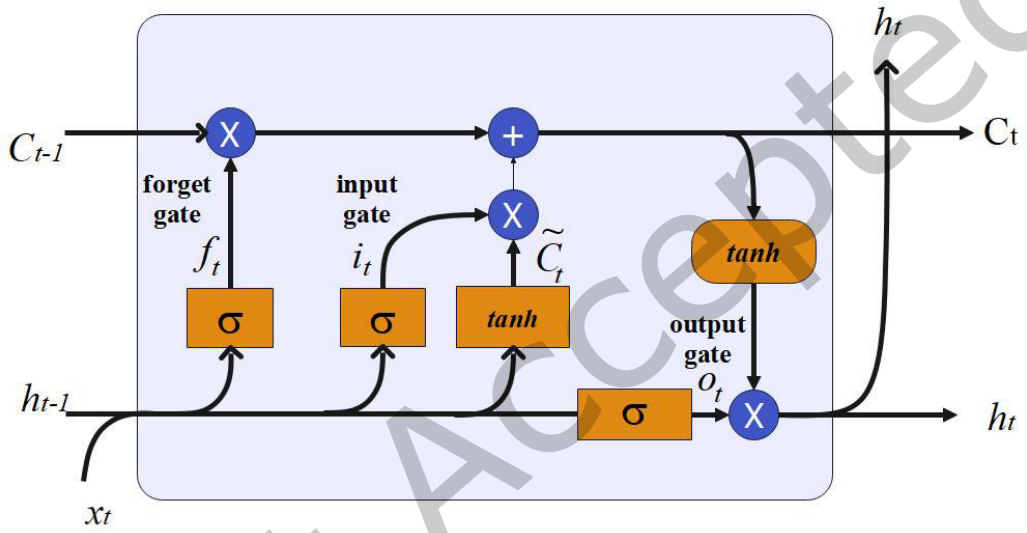


Figure 9: Structure of a LSTM network

Various notations are employed to illustrate the model, as demonstrated below:

$i_t \rightarrow input\ gate$
$f_t \rightarrow forget\ gate$
$o_t \rightarrow output\ gate$
$\sigma \rightarrow sigmoid\ function$
$w_x \rightarrow weight\ for\ the\ respective\ gate\ (x)$
$h_{t-1} \rightarrow output\ of\ the\ (t-1)\ timestamp$
$x_t \rightarrow currentinput(attimestampt)$
$b_x \rightarrow biases\ for\ the\ respective\ gates\ (x)$

The cell state in the LSTM unit is like a memory bank. It decides what to remember, what to forget, and what new information to include based on the current input. The forgetting gate performs a specialized function akin to a gatekeeper. It selectively retains data adhering to stringent algorithmic criteria while promptly discarding any information that falls short of these criteria. This strategic mechanism adeptly addresses the intricate challenge of handling long-term dependencies within the model. A sigmoid function (showed in Equation 11) comes into play to facilitate this decision-making process. This function produces an output that typically falls within the range of 0 to 1, with the outcome often leaning toward either 0 or 1 in most instances. Here "0" signifies that the gate is completely obstructing any passage, while a "1" indicates that the gates are permitting unrestricted passage. The operation involves computing the dot product of *h(t-1)* and *x(t)* and utilizing the sigmoid function, as described in Equation 12. This process yields a value ranging from 0 to 1 for each element in the cell state *C(t-1)*. When the output is '1', it indicates retention, whereas '0' signifies complete forgetting.

$$\sigma(x) = \frac{1}{1+e^{-x}} \quad (11)$$

$$f_t = \sigma\left(w_f \cdot [h_{t-1}, x_t] + b_f\right) \quad (12)$$

The input gate oversees the process of incorporating information at the current time step. The input gate functions through a sequence of three key stages. A sigmoid layer evaluates which values should be updated. (showed in Equation 13). 2. An activation function layer, utilizing hyperbolic tangent, generates a vector of potential new values, Č(t), that could augment the current state (showed in Equation 14). These two outputs, *i(t)* * Č(t), are combined to perform an update on the cell state, resulting in the new cell state C(t) (showed in Equation 15).

$$i_t = \sigma(w_i \cdot [h_{t-1}, x_t] + b_i) \quad (13)$$

$$\check{C}_t = tanh(w_C \cdot [h_{t-1}, x_t] + b_C) \quad (14)$$

$$C_t = f_t C_{t-1} + i_t \check{C}_t \quad (15)$$

The output gate exerts control over the filtered output derived from the current unit state. Initially, a sigmoid layer determines the portions of the cell state to be extracted (Equation 16). Subsequently, the cell state undergoes a hyperbolic tan transformation to confine its values within the range of -1 to 1, and this result is multiplied by the sigmoid gate's output (Equation 17)

$$o_t = \sigma(w_o \cdot [h_{t-1}, x_t] + b_o) \quad (16)$$

$$h_t = o_t \times tanh(C_t) \quad (17)$$

This multi-gate architecture in LSTM networks empowers them to capture and utilize long-range dependencies more effectively compared to alternative methods. Furthermore, the LSTM architecture incorporates a dropout layer, an integral component in its design. This layer introduces an element of randomness during the training process by temporarily excluding specific neural network cells from the

network. This deliberate infusion of randomness serves a crucial role, mitigating the risk of overfitting and bolstering the network's overall resilience and adaptability.

In our model, we focus on predicting methane concentration in mine atmosphere within an underground coal mine. In the task of forecasting methane concentrations in a mine, the input factor matrix *M*, with dimensions $H \times F$ where $H$ =24 *hours*, represents the past 24 hours of hourly data, and $F$=3 includes three input parameters: methane concentration, temperature, and humidity. This 24×3 matrix is structured such that each row corresponds to data from one hour in the past, and each column is dedicated to one of the features. A conceptual illustration of how the matrix *M* might look with historical data from $H$=24 and $F$=3 is given as follows.

$$M = \begin{bmatrix} CH_4(t-1) & Temp(t-1) & Hum(t-1) \\ CH_4(t-2) & Temp(t-2) & Hum(t-2) \\ \vdots & \vdots & \vdots \\ CH_4(t-24) & Temp(t-24) & Hum(t-24) \end{bmatrix}$$

The final output layer of our model provides the predicted target, represented as $\acute{y}_{1,t}$ while the corresponding observed value is denoted as $y_{1,t}$. In the design of this model, the forecasting horizon extends up to 2 hours into the future, denoted as the lead, allowing it to predict methane concentration up to t+2 timesteps. The model considers a lag of 24 hours, incorporating data up to t-24 for the forecasting process. Throughout the training process, the LSTM model utilizes the 'Adam' optimization algorithm as optimization function and mean absolute error (MAE) as training loss function. A summary of the parameters utilized in the proposed LSTM-based forecasting model is presented in Table 4.

Table 4: Summary of the forecasting model parameters

| variables | value |
|---|---|
| Number of hidden neurons | 150 |
| Epochs | 1500 |
| Recurrent connections' activation function | Sigmoid |
| Output activation function | Hyperbolic tangent (tanh) |
| Optimizer | Adam |
| Loss function of training | MAE |
| Number of forward forecast points | 2 |

The method employs the Root Mean Square Error (RMSE) as validation parameter to assess forecasting accuracy. A lower RMSE indicates higher prediction accuracy, as it signifies smaller differences between forecasts and original values. RMSE is calculated for each sequence and compared among the models being studied. The RMSE can be computed using the formula provided below.

$$RMSE = \sqrt{\frac{1}{n}\sum_{t=1}^{n}\left(\acute{y}_{1,t} - y_{1,t}\right)^2} \qquad (18)$$

Before using the actual dataset, we validate our model with artificial data. Sine function is used to generate artificial data. The function, used as the input of the LSTM model, is represented as below (Equation 19).

$$y = sin\left(\frac{t}{5\pi}\right) + 6 \quad (19)$$

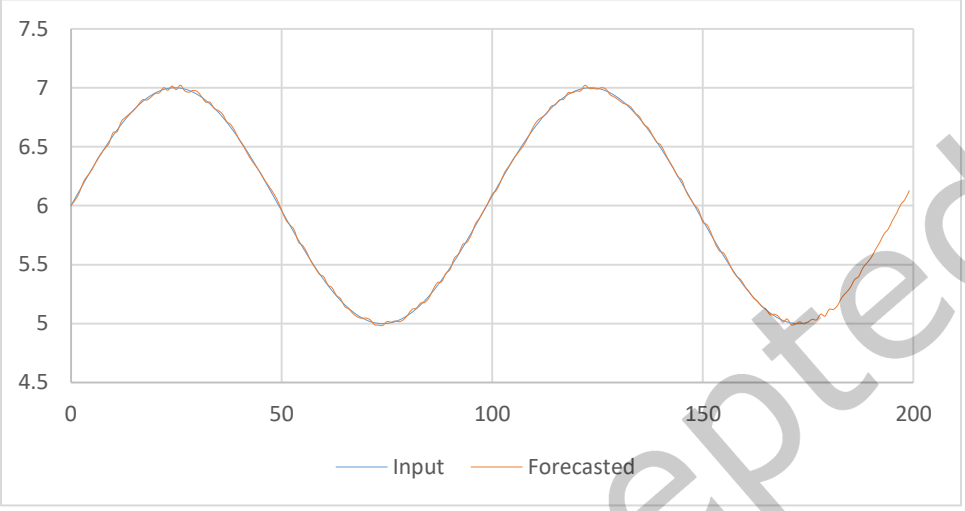


Figure 10: Artificial Input data and output forecasted by the model.

The input function and the forecasted output is shown in Figure 10 that aims a validation of our proposed model for the given input.

The actual dataset collected from the mine, presented in Table 3 includes both time and date components. To prepare this data for training the model, the time and date data are consolidated into a single timestamp format. Additionally, the values of methane concentration, temperature, and humidity are normalized to facilitate more effective model training. It's worth noting that data is collected from three distinct locations within the mine, and each of these three datasets is employed separately for model training. In this process, 70% of the data is allocated for training, while the remaining 30% is reserved for model validation.

### 3.5 Establishment of a Cloud-Based Monitoring and Alert System

The IIoT devices strategically positioned within the underground coal mine are equipped to measure crucial parameters such as methane concentration, temperature, and humidity. These devices employ the MQTT protocol to transmit the gathered data over the internet to an MQTT broker hosted on Amazon Web Services (AWS) cloud. An MQTT broker, (Mosquitto) has been set up on an AWS EC2 instance to facilitate this data transfer. Our designed LSTM-based forecasting model has also deployed within AWS EC2, operationalized using Flask, a Python-based micro-framework ideal for small-scale model

deployment. This model is adept at predicting methane concentrations based on historical data encompassing the past 24 hours, providing forecasts for the upcoming 2 hours.

To offer convenient real-time data visualization and access through both a mobile application and a web-based dashboard, the Cayenne IoT cloud platform, developed by *myDevices* is used. This platform also facilities MQTT for efficient data transmission. The deployed IIoT devices seamlessly relay real-time data to Cayenne in addition to AWS. The real-time data are transmitted to the cloud every 30 seconds. Meanwhile, for local warnings, the IIoT device captures data every second and compares it to the statutory methane concentration limit of 1.25%. Moreover, the 2-hour methane concentration predictions generated by the Flask-deployed model are transmitted by the MQTT broker to the Cayenne cloud, thereby enabling monitoring through a mobile app or web-based interface. In cases where methane concentration surpasses the statutory limit, a SMS alert is promptly dispatched to the mine manager. Furthermore, the MQTT broker reciprocally communicates the forecasted data back to the IIoT device, empowering it to issue alerts when the forecasted values exceed the statutory limit. The buzzer issues a continuous beep for methane levels over 1.25% and a rhythmic beep at every 5 seconds if forecasted levels exceed this threshold, providing vigilant warnings. A visual representation of the comprehensive monitoring and warning system is illustrated through a flowchart in figure 11.

## 4 Results and Discussions

The results of this study are presented and discussed in a sequential manner, highlighting various aspects of the study.

### 4.1 Model Training and Evaluation

Training and testing of the LSTM model involved utilizing the dataset, which comprises underground coal mining data collected by the specially developed IIoT device. This data originates from three specific mine locations: the coal mining face, the outbye side of the current mining panel, and the main return airway. The Figure 12 illustrates how the Mean Absolute Error (MAE) evolves over the course of training as a function of the number of training epochs.

To assess the model's forecasting performance for methane concentration, it's essential to compare the actual and predicted values. This comparison provides valuable insights into the model's predictive capabilities. The comparison is visually depicted in Figure 13-15 for location 1-3 respectively while Figure 16 illustrated the absolute error values for location 1.

### 4.2 Comparative Analysis of the Proposed Model

Alongside LSTM, this training conducted on the multivariate Multilayer Perceptron (MLP), Vector autoregression (VAR) and Auto-Regressive Integrated Moving Average (ARIMA) models. To assess and compare these models' performance, the RMSE error is employed as a key parameter. As depicted in Figure 17-19 and Table 5, the results of this comparative evaluation highlight the superior performance of the LSTM model, particularly in terms of the mean absolute error (MAE), mean absolute percentage error (MAPE) and root mean square error (RMSE).

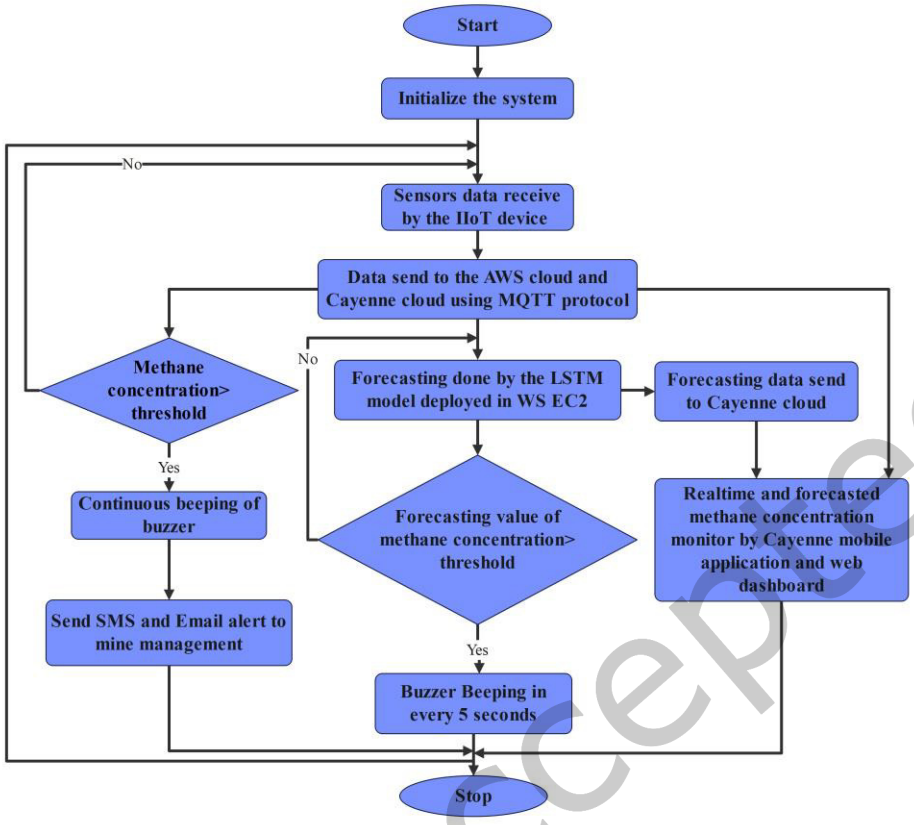


Figure 11: Flow Chart for IIoT Based Forecasting, Monitoring and Warning System.

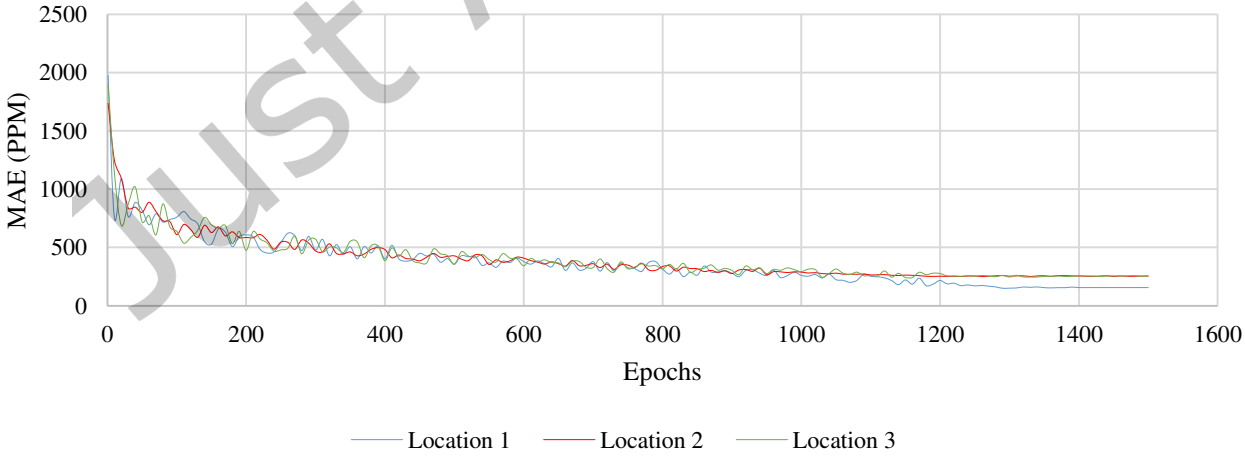


Figure 12: MAE over epochs during training

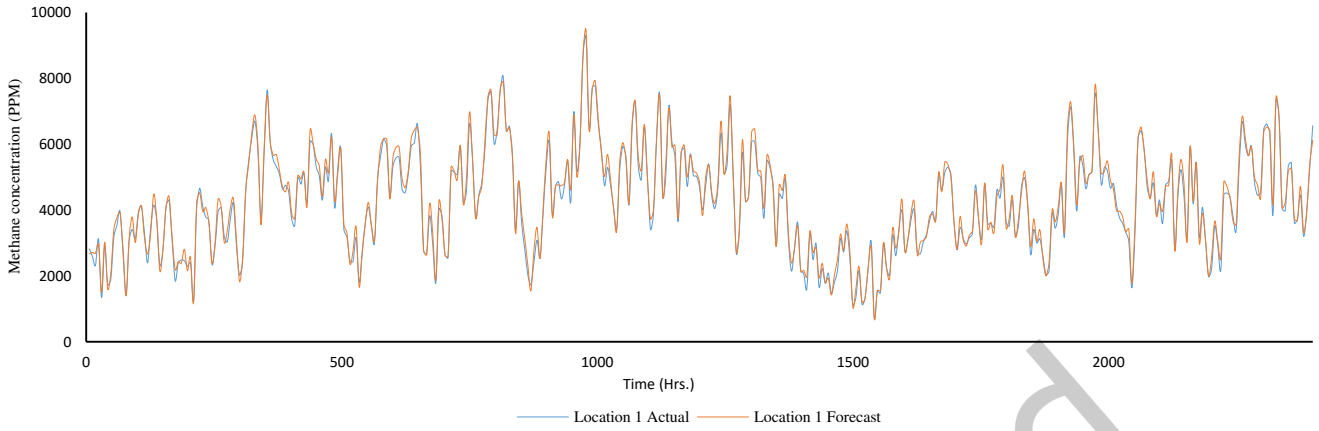


Figure 13: Graphical Comparison of Actual Methane Concentration vs. Forecasted for Location 1

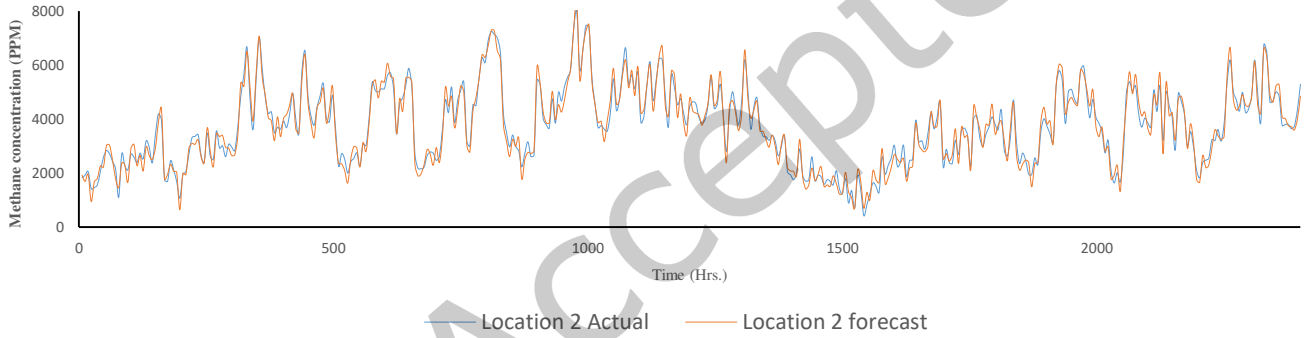


Figure 14: Graphical Comparison of Actual Methane Concentration vs. Forecasted for Location 2

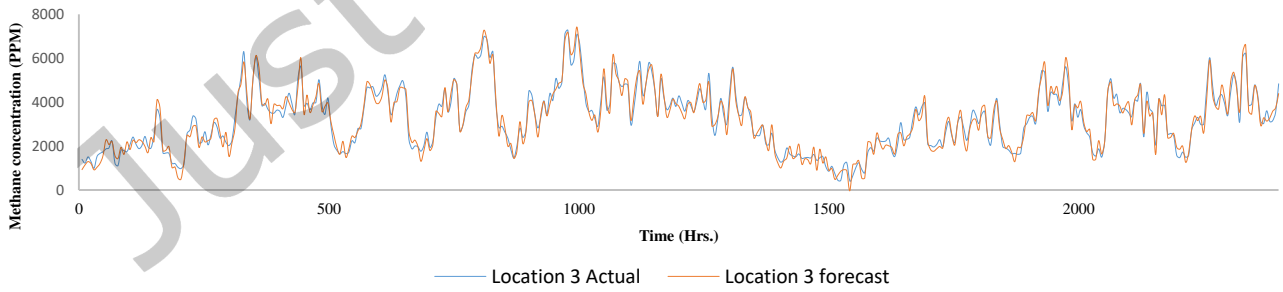


Figure 15: Graphical Comparison of Actual Methane Concentration vs. Forecasted for Location 3

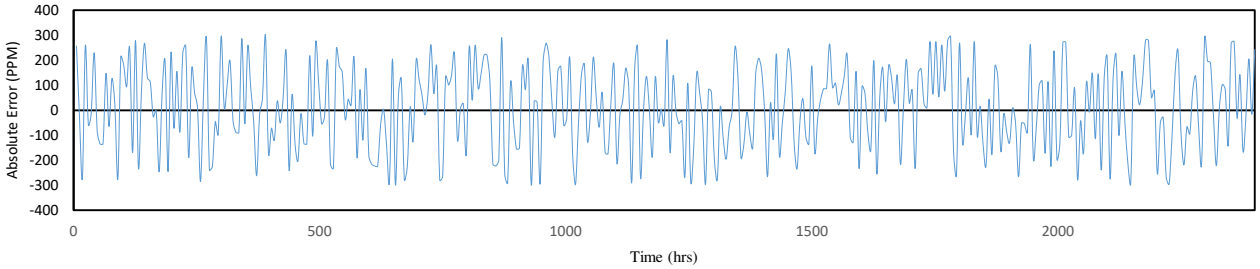


Figure 16: Absolute Error of Forecasting Methane concentration at Location 1

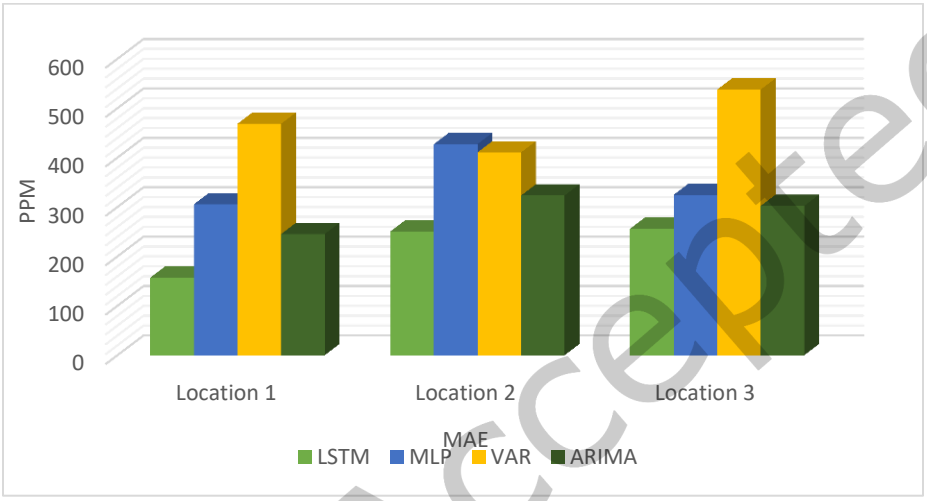


Figure 17: MAE for LSTM, MLP, VAR and ARIMA Forecasting

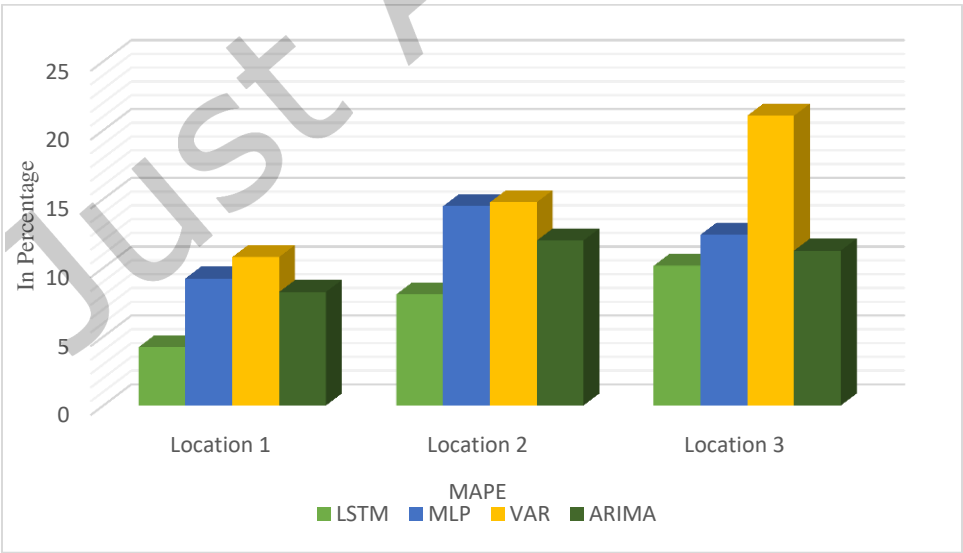

Figure 18: MAPE for LSTM, MLP, VAR and ARIMA Forecasting

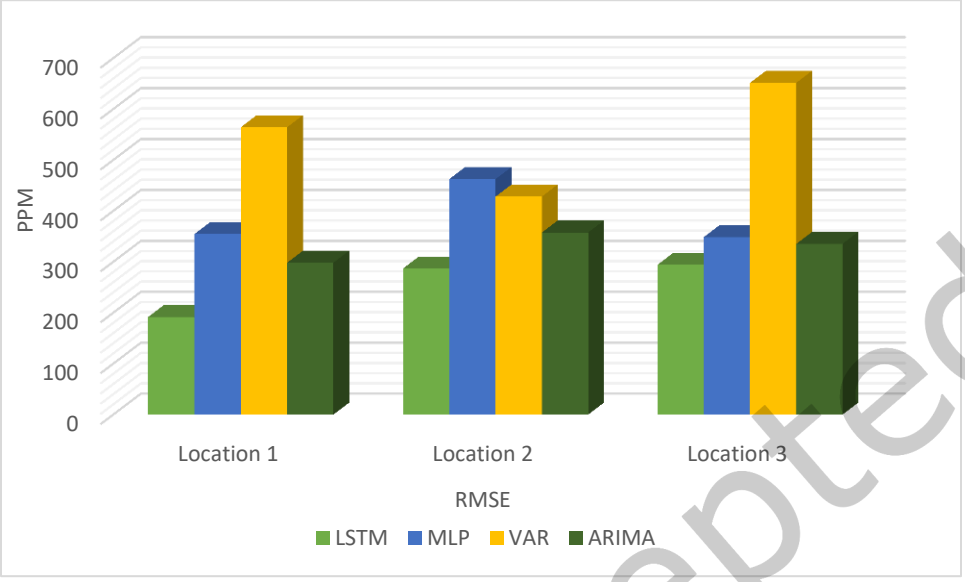


Figure 19: RMSE for LSTM, MLP, VAR and ARIMA Forecasting

Table 5: MAE, MAPE and RMSE for LSTM, MLP, VAR and ARIMA

| | Location 1 | | | Location 2 | | | Location 3 | | |
|---|---|---|---|---|---|---|---|---|---|
| | MAE (ppm) | MAPE (%) | RMSE (ppm) | MAE (ppm) | MAPE (%) | RMSE (ppm) | MAE (ppm) | MAPE (%) | RMSE (ppm) |
| LSTM | 156.95 | 4.23 | 191.53 | 250.30 | 8.07 | 286.82 | 255.89 | 10.15 | 294.31 |
| MLP | 305.45 | 9.23 | 354.54 | 427.21 | 14.48 | 462.60 | 324.46 | 12.40 | 348.54 |
| VAR | 468.48 | 10.78 | 564.25 | 410.47 | 14.76 | 428.26 | 537.65 | 21.05 | 651.54 |
| ARIMA | 245.25 | 8.24 | 298.25 | 323.25 | 11.98 | 357.68 | 302.18 | 11.25 | 335.25 |

It's worth noting that the dataset from the coal mining face (Location 1) exhibited the lowest error among all the scenarios tested. The overall results suggest that the LSTM model is the more accurate than MLP, VAR and ARIMA models in predicting the variables of interest within the coal mining environment.

### 4.3 IIoT-Cloud Integration and Monitoring System

The study also integrated an Industrial Internet of Things (IIoT) device with AWS and the Cayenne cloud platform to enable comprehensive real-time and forecasted data monitoring. Users can access this

monitoring through both a mobile application and a web-based dashboard, as glimpsed in Figure 20 (a) and 20 (b) respectively. This integration provides a valuable tool for enhancing safety and operational efficiency within the coal mining operation.

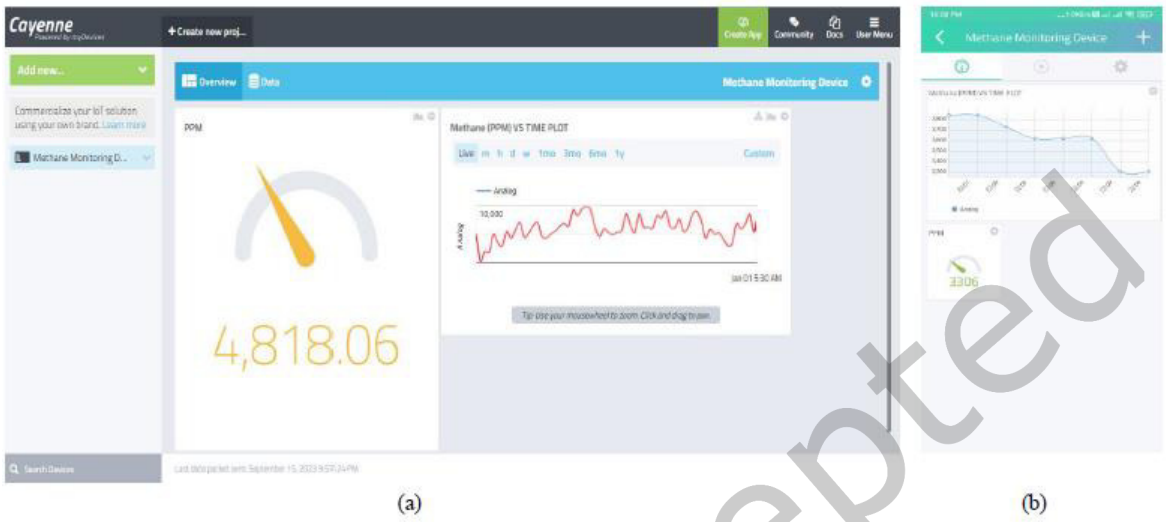


Figure 20: Snapshot of (a) Cayenne Web Dashboard, (b) Android Application Interface

The study's findings from the subsection of the results suggest that the LSTM model is effective in predicting key variables within the coal mining environment. The integration of IIoT technology with cloud platforms offers real-time monitoring and alerts, which can play a crucial role in ensuring the safety and productivity of mining operations. These results hold significant implications for the mining industry, where accurate prediction and monitoring are essential for operational success.

## 5 Conclusions

This study has concentrated on real-time methane monitoring and forecasting in underground coal mines, aligning with Industry 4.0 principles. An IIoT device designed for this purpose collects training data from underground mines, recording key parameters like methane concentration, temperature, and humidity. Using this data, a multivariate forecasting model based on LSTM technology has been trained and later deployed in the cloud. Field experiments have been conducted at a site operated by Eastern Coalfields Limited in India. Once deployed, the IIoT device continuously transmits real-time data to the cloud. The model processes this data and sends back results to the device. If methane levels exceed predefined thresholds, the device issues warnings for both real-time and forecasted concentrations. These forecasts, together with real-time data, are made available via mobile apps and a web dashboard. The model's accuracy has been evaluated using mean absolute error (MAE), mean absolute percentage error (MAPE), and root mean square error (RMSE). For Location 1, our proposed LSTM based model achieved the following results: MAE of 156.95 ppm, MAPE of 4.23%, and RMSE of 191.53 ppm. In comparison, the Multilayer Perceptron (MLP) model had an MAE of 305.45 ppm, a MAPE of 9.23%, and an RMSE of 354.54

ppm. The Vector Autoregression (VAR) model showed an MAE of 468.48 ppm, a MAPE of 10.78%, and an RMSE of 564.25 ppm. The Auto-Regressive Integrated Moving Average (ARIMA) model yielded an MAE of 245.25 ppm, a MAPE of 8.24%, and an RMSE of 298.25 ppm. This comparative analysis demonstrates that the LSTM model significantly outperforms the MLP, VAR, and ARIMA models, delivering superior performance. Similar results are observed for Locations 2 and 3, where the developed LSTM model also outperformed the other models. The IIoT device can be utilized in other industrial settings where there is a risk of gas leakage. However, its current application is limited to forecasting only methane gas levels. To ensure safety of mine environment, other safety parameters such as dust concentration, oxygen levels, and carbon monoxide levels can also be considered. As a future research direction, a forecasting device could be developed, incorporating these various safety parameters to enhance overall safety.

**References**


[1] M.J. McPherson. 2009. Subsurface Ventilation Engineering. Fresno: Mine Ventilation Services Inc.

[2] Hal Sider. 1983. Safety and productivity in underground coal mining. The Review of Economics and Statistics (1983), 225–233.

[3] Marian Gieras, Rudolf Klemens, Grzegorz Rarata, and Piotr Wolański. 2006. Determination of explosion parameters of methane-air mixtures in the chamber of 40 dm3 at normal and elevated temperature. Journal of Loss Prevention in the Process Industries 19, 2–3 (2006), 263–270.

[4] Soumyadeep Paty and Supreeti Kamilya. 2022. Identification of rock images in mining industry: an application of deep learning technique. In International Conference on Advances in Data Science and Computing Technologies, Springer, 235–242.

[5] Soumyadeep Paty. 2024. IIoT Based Smart Water Quality Monitoring for Sustainable Mining Practices in the Industry 4.0 Era. In Water Informatics: Challenges and Solutions Using State of Art Technologies, Springer, 221-235.

[6] Jiang Tiantian and Yang Zhanyong. 2011. Research on mine safety monitoring system based on WSN. Procedia Engineering 26, (2011), 2146–2151.

[7] Xiaodong Wang, Xiaoguang Zhao, Zize Liang, and Min Tan. 2007. Deploying a wireless sensor network on the coal mines. In 2007 IEEE international conference on networking, sensing and control, IEEE, 324–328.

[8] Long Shi, Jinhui Wang, Guomin Zhang, Xudong Cheng, and Xianbo Zhao. 2017. A risk assessment method to quantitatively investigate the methane explosion in underground coal mine. Process Safety and Environmental Protection 107, (2017), 317–333.

[9] Xiaoguang Niu, Xi Huang, Ze Zhao, Yuhe Zhang, Changcheng Huang, and Li Cui. 2007. The design and evaluation of a wireless sensor network for mine safety monitoring. In IEEE GLOBECOM 2007-IEEE Global Telecommunications Conference, IEEE, 1291–1295.

[10] Qi Mu, Tanghong Wang, and Yikai Jia. 2015. Research on framework of underground wearable devices framework based on cloud computing. In 2015 8th International Symposium on Computational Intelligence and Design (ISCID), IEEE, 458–461.

[11] Mohammad Ali Moridi, Youhei Kawamura, Mostafa Sharifzadeh, Emmanuel Knox Chanda, Markus Wagner, Hyongdoo Jang, and Hirokazu Okawa. 2015. Development of underground mine monitoring and communication system integrated ZigBee and GIS. International Journal of Mining Science and Technology 25, 5 (2015), 811–818.

[12] DP Creedy. 1993. Methane emissions from coal related sources in Britain: Development of a methodology. Chemosphere 26, 1–4 (1993), 419–439.

[13] David A Kirchgessner, Stephen D Piccot, and Sushma S Masemore. 2000. An improved inventory of methane emissions from coal mining in the United States. Journal of the Air & Waste Management Association 50, 11 (2000), 1904–1919.

[14] Sello Mathatho, Pius Adewale Owolawi, and Chunling Tu. 2020. An artificial neural network and principle component analysis based model for methane level prediction in underground coal mines. In Proceedings of the 2nd international conference on intelligent and innovative computing applications, 1–7.

[15] Yongkang Yang, Qiaoyi Du, Chenlong Wang, and Yu Bai. 2020. Research on the method of methane emission prediction using improved grey radial basis function neural network model. Energies 13, 22 (2020), 6112.

[16] Xiaoyu Yi, Jun Wu, Gaolei Li, Ali Kashif Bashir, Jianhua Li, and Ahmad Ali AlZubi. 2022. Recurrent semantic learning-driven fast binary

vulnerability detection in healthcare cyber physical systems. IEEE Transactions on Network Science and Engineering 10, 5 (2022), 2537–2550.

[17] Animesh Ghosh, Bikas Mondal, Santu Mondal, Tanmoy Hazra, and Arindam Biswas. 2023. Development of Resistive-type IoT-Based Methane Gas Concentration Transmitter Using SnO2 Material. Journal of The Institution of Engineers (India): Series D 104, 2 (2023), 515–529.

[18] Long Shi, Jinhui Wang, Guomin Zhang, Xudong Cheng, and Xianbo Zhao. 2017. A risk assessment method to quantitatively investigate the methane explosion in underground coal mine. Process Safety and Environmental Protection 107, (2017), 317–333.

[19] Alana K Ayasse, Andrew K Thorpe, Dar A Roberts, Christopher C Funk, Philip E Dennison, Christian Frankenberg, Andrea Steffke, and Andrew D Aubrey. 2018. Evaluating the effects of surface properties on methane retrievals using a synthetic airborne visible/infrared imaging spectrometer next generation (AVIRIS-NG) image. Remote sensing of environment 215, (2018), 386–397.

[20] Nikodem Szlązak, Dariusz Obracaj, and Justyna Swolkień. 2020. Enhancing safety in the Polish high-methane coal mines: An overview. Mining, Metallurgy & Exploration 37, 2 (2020), 567–579.

[21] Zygmunt Łukaszczyk and Henryk Badura. 2022. Analysis of forecasted methane concentration at the top gate of a wall ventilated by means of the "U" system. Case study. Management Systems in Production Engineering 30, 4 (2022), 342–347.

[22] C Özgen Karacan. 2008. Modeling and prediction of ventilation methane emissions of US longwall mines using supervised artificial neural networks. International Journal of Coal Geology 73, 3–4 (2008), 371–387.

[23] C Özgen Karacan, Felicia A Ruiz, Michael Cotè, and Sally Phipps. 2011. Coal mine methane: a review of capture and utilization practices with benefits to mining safety and to greenhouse gas reduction. International journal of coal geology 86, 2–3 (2011), 121–156.

[24] HF Coward. 1952. Limit of inflammability of Gases and Vapors. Bur. Mines Bull 503, (1952), 155.

[25] Evgeny E Karpov, Evgeny F Karpov, Alexey Suchkov, Sergey Mironov, Alexander Baranov, Vladimir Sleptsov, and Lucia Calliari. 2013. Energy efficient planar catalytic sensor for methane measurement. Sensors and Actuators A: Physical 194, (2013), 176–180.

[26] Dongping Xue, Pengtao Wang, Zhanying Zhang, and Yan Wang. 2019. Enhanced methane sensing property of flower-like SnO2 doped by Pt nanoparticles: A combined experimental and first-principle study. Sensors and Actuators B: Chemical 296, (2019), 126710.

[27] Vincenza Portosi, Dario Laneve, Mario Christian Falconi, and Francesco Prudenzano. 2019. Advances on photonic crystal fiber sensors and applications. Sensors 19, 8 (2019), 1892.

[28] Lionel Tombez, Eric J Zhang, Jason S Orcutt, Swetha Kamlapurkar, and William MJ Green. 2017. Methane absorption spectroscopy on a silicon photonic chip. Optica 4, 11 (2017), 1322–1325.

[29] Michal Nikodem, Genevieve Plant, David Sonnenfroh, and Gerard Wysocki. 2015. Open-path sensor for atmospheric methane based on chirped laser dispersion spectroscopy. Applied Physics B 119, (2015), 3–9.

[30] Zipeng Zhu, Yuhui Xu, and Binqing Jiang. 2012. A one ppm NDIR methane gas sensor with single frequency filter denoising algorithm. Sensors 12, 9 (2012), 12729–12740.

[31] Ian F Akyildiz and Erich P Stuntebeck. 2006. Wireless underground sensor networks: Research challenges. Ad Hoc Networks 4, 6 (2006), 669–686.

[32] Mo Li and Yunhao Liu. 2007. Underground structure monitoring with wireless sensor networks. In Proceedings of the 6th international conference on Information processing in sensor networks, 69–78.

[33] Ankur Dumka, Sandip K Chaurasiya, Arindam Biswas, and Hardwari Lal Mandoria. 2019. A complete guide to wireless sensor networks: from inception to current trends. CRC Press.

[34] Byung Wan Jo, Rana Muhammad Asad Khan, and Omer Javaid. 2019. Arduino-based intelligent gases monitoring and information sharing Internet-of-Things system for underground coal mines. Journal of Ambient Intelligence and Smart Environments 11, 2 (2019), 183–194.

[35] Ankita Ray Chowdhury, Ankita Pramanik, and Gopal Chandra Roy. 2023. IoT and LoRa based smart underground coal mine monitoring system. Microsystem Technologies 29, 7 (2023), 919–938.

[36] Yaqin Wu, Mengmeng Chen, Kai Wang, and Gui Fu. 2019. A dynamic information platform for underground coal mine safety based on internet of things. Safety science 113, (2019), 9–18.

[37] Arif Hussain Soomro and Muhammad Taha Jilani. 2020. Application of IoT and artificial neural networks (ANN) for monitoring of underground

coal mines. In 2020 international conference on information science and communication technology (ICISCT), IEEE, 1–8.

[38] R. Jagadeesh, and R. Nagaraja. 2017. IoT Based Smart Helmet for Unsafe Event Detection for Mining Industry. Int Res J Eng Technol, 4, no. 1 (2017), 1487-1491. Retrieved from https://www.irjet.net/archives/V4/i1/IRJET-V4I1289.pdf.

[39] Maviya Noorin and KV Suma. 2018. IoT based wearable device using WSN technology for miners. In 2018 3rd IEEE international conference on recent trends in electronics, information & communication technology (RTEICT), IEEE, 992–996.

[40] CJ Behr, Anuj Kumar, and Gerhard P Hancke. 2016. A smart helmet for air quality and hazardous event detection for the mining industry. In 2016 IEEE International Conference on Industrial Technology (ICIT), IEEE, 2026–2031.

[41] J. C. Diaz, Z. Agioutantis, S. Schafrik, and D. T. Hristopulos. 2021. Mine Ventilation (1st ed.). Towards Atmospheric Monitoring Data Analysis in Underground Coal Mines, 498–506. CRC Press. https://doi.org/10.1201/9781003188476.

[42] Z Agioutantis, K Luxbacher, M Karmis, and S Schafrik. 2014. Development of an atmospheric data-management system for underground coal mines. Journal of the Southern African Institute of Mining and Metallurgy 114, 12 (2014), 1059–1063

[43] Eugeniusz Krause. 2015. Short-term predictions of methane emissions during longwall miting. Archives of Mining Sciences 60, 2 (2015), 581–594.

[44] AP Niewiadomski and H Badura. 2019. Evaluation of a one-day average methane concentrations forecast at the outlet from the longwall ventilation region as tool of supporting selection of methane prevention measures. In Topical Issues of Rational Use of Natural Resources 2019, Volume 1. CRC Press, 88–99.

[45] ByungWan Jo and Rana Muhammad Asad Khan. 2018. An internet of things system for underground mine air quality pollutant prediction based on azure machine learning. Sensors 18, 4 (2018), 930.

[46] Henryk Badura. 2022. Analysis of one-day forecasts of the maximum methane concentration in a tailgate of a longwall ventilated with U system-a case study. Mining Machines 40, (2022).

[47] AP Niewiadomski, H Badura, and G Pach. 2021. Recommendations for methane prognostics and adjustment of short-term prevention measures based on methane hazard levels in coal mine longwalls. In E3S Web of Conferences, EDP Sciences, 08001, 2021.

[48] S Espressif. 2017. Esp32 datasheet. IotY Based Microcontroller (2017).